Prediction of Reader Estimates of Mammographic Density using Convolutional Neural Networks

Georgia V. Ionescu[a], Martin Fergie[b], Michael Berks[b,d], Elaine F. Harkness[b,c,f], Johan Hulleman[d], Adam R. Brentnall[e], Jack Cuzick[e], D. Gareth Evans[f,g,h], Susan M. Astley[b,c,f,*]

[a]School of Computer Science, University of Manchester, Stopford Building, Oxford Road, Manchester, UK
[b]Division of Informatics, Imaging and Data Sciences, Faculty of Biology, Medicine and Health, University of Manchester, Stopford Building, Oxford Road, Manchester, UK
[c]The University of Manchester, Manchester Academic Health Science Centre, Manchester NHS Foundation Trust, Manchester, UK
[d]School of Biological Sciences, Division of Neuroscience and Experimental Psychology, University of Manchester, Manchester, UK
[e]Centre for Cancer Prevention, Wolfson Institute of Preventive Medicine, Queen Mary University of London, London EC1M 6BQ, UK
[f]Prevent Breast Cancer and Nightingale Breast Screening Centre, Manchester University NHS Foundation Trust, Manchester Academic Health Science Centre, Southmoor Road, Wythenshawe, Manchester M23 9LT, UK
[g]The Christie NHS Foundation Trust, Manchester Academic Health Science Centre, Withington, Manchester M20 4BX, UK
[h]Genomic Medicine, Division of Evolution and Genomic Science, Manchester Academic Health Sciences Centre, University of Manchester and Manchester University NHS Foundation Trust, Manchester M13 9WL, UK

Abstract.
Background: Mammographic density is an important risk factor for breast cancer. In recent research, percentage density assessed visually using Visual Analogue Scales (VAS) showed stronger risk prediction than existing automated density measures, suggesting readers may recognise relevant image features not yet captured by hand-crafted algorithms. With deep learning, it may be possible to encapsulate this knowledge in an automatic method.
Method: We have built convolutional neural networks (CNN) to predict density VAS scores from full-field digital mammograms. The CNNs are trained using whole-image mammograms, each labelled with the average VAS score of two independent readers. Each CNN learns a mapping between mammographic appearance and VAS score so that at test time, they can predict VAS score for an unseen image. Networks were trained using 67520 mammographic images from 16968 women and for model selection we used a dataset of 73128 images. Two case-control sets of contralateral mammograms of screen detected cancers and prior images of women with cancers detected subsequently, matched to controls on age, menopausal status, parity, HRT and BMI, were used for evaluating performance on breast cancer prediction.
Results: In the case-control sets, odds ratios of cancer in the highest *vs* lowest quintile of percentage density were 2.49 (95 %CI: 1.59 - 3.96) for screen detected cancers and 4.16 (2.53 - 6.82) for priors, with matched concordance indices of 0.587 (0.542 - 0.627) and 0.616 (0.578 - 0.655) respectively. There was no significant difference between reader VAS and predicted VAS for the prior test set (likelihood ratio chi square, p=0.134).
Conclusion: Our fully automated method shows promising results for cancer risk prediction and is comparable with human performance.

Keywords: breast cancer, mammographic density, deep learning, risk, VAS.

*Susan M. Astley, sue.astley@manchester.ac.uk

1 Introduction

Mammographic density is one of the most important independent risk factors for breast cancer and can be defined as the relative proportion of radio-dense fibroglandular tissue to radio-lucent fatty tissue in the breast, as visualised in mammograms. Women with dense breasts have a 4-6 fold increased risk of breast cancer compared to women with fatty breasts,[1] and breast density has been shown to improve the accuracy of current risk prediction models.[2] The reliable identification of women at increased risk of developing breast cancer paves the way for the selective implementation of risk-reducing interventions.[3] Additionally, dense tissue may mask cancers, reducing the sensitivity of mammography,[4] and breast cancer mortality can be reduced if women at high risk are identified early and treated adequately.[5] There is international interest in personalizing breast screening so that women with dense breasts are screened more regularly or with alternative or supplemental modalities.[6]

A number of methods have been used to measure mammographic density (MD). These include visual area-based methods, for example BI-RADS breast composition categories,[7] Boyd categories,[8] percent density recorded on Visual Analogue Scales (VAS)[9] and semi-automated thresholding (Cumulus).[10] The automated Densitas software[11] operates in an area-based fashion on processed (*for presentation*) full field digital mammograms (FFDM), whilst methods including Volpara[12] and Quantra[13] use raw (*for processing*) mammograms to estimate volumes of dense fibroglandular and fatty tissue in the breast. Density measures may be expressed in absolute terms (area or volume of dense tissue) or more commonly as a percentage expressing the relative proportion of dense tissue in the breast. Recent studies have investigated the relationship between

breast density and the risk of breast cancer and found differences depending on the density method used.[14,15]

Subjective assessment of percentage density recorded on VAS has a strong relationship with breast cancer risk.[16] In a recent case-control study[14] with three matched controls for each cancer (366 detected in the contralateral breast at screening on entry to the study and 338 detected subsequently), the odds ratio for screen detected cancers in the contralateral breast in the highest compared to the lowest quintile of percentage density using VAS was 4.37 (95% CI: 2.72 - 7.03) compared to 2.42 (95% CI: 1.56 - 3.78) and 2.17 (95% CI: 1.41 - 3.33) for Volpara and Densitas percent density respectively. Similar results were found for subsequent cancers, with odds ratios of 4.48 (95% CI: 2.79 - 7.18) for VAS, 2.87 (95% CI: 1.77 - 4.64) for Volpara and 2.34 (95% CI: 1.50 - 3.68) for Densitas. This suggests that expert readers might recognise important features present in the mammographic images of high-risk women which existing automated methods may miss. In part this may be due to their assessment of patterns of density as well as quantity of dense tissue; there is already evidence in the same case-control setting that explicit quantification of density patterns adds independent information to percent density for risk prediction.[17] However, visual assessment of density is time consuming and significant reader variability has been observed.[18,19]

There have been numerous attempts to automate density assessment using computer vision algorithms[20–22] that require hand-crafted descriptive features and prior knowledge of the data. Conversely, deep learning techniques extract and learn relevant features directly from the data, without prior knowledge.[23] Convolutional neural networks (CNN) have been successfully used for a wide range of imaging tasks including image classification,[24] object detection and semantic segmenta-

tion,[25] and organ classification in medical images.[26] In mammography, deep learning has been used for breast segmentation,[27] breast lesion detection,[28] breast mass detection[29,30] and breast mass segmentation.[30] Various deep learning approaches have been proposed for other breast cancer related tasks such as differentiation between benign and malignant masses[31] and discrimination between masses and microcalcifications.[32]

Deep learning methods for estimating mammographic density have gained increased attention in recent years, however the number of published studies is low. Petersen et al[33] were amongst the first to propose unsupervised deep learning, using a multiscale denoising autoencoder to learn an image representation to train a machine learning model to estimate breast density. Following Petersen's study, Kallenberg et al.[34] proposed a variant of the autoencoder that learns a sparse overcomplete representation of the features, achieving an ROC AUC of 0.61 for breast cancer risk prediction. A more recent study employed supervised deep learning to classify breast density into BI-RADS categories and to differentiate between scattered density and heterogeneously dense breasts, showing promising results.[35] As VAS has been shown to be a better predictor of cancer than other automated methods, we developed a method of breast density estimation by predicting VAS scores using a supervised deep learning approach that learns features associated with breast cancer. The aim of this study is to create an automated method with the potential to match human performance on breast cancer risk assessment. Our model predicts mammographic density VAS scores with the final goal of assessing breast cancer risk.

2 Data

We used data from the Predicting Risk Of Cancer At Screening (PROCAS) study.[36] 57,902 women were recruited to PROCAS between October 2009 and March 2015, with full-field digital mammograms available for 44,505. Density was assessed by expert readers using VAS as described in Section 3.1. Data from women who had cancer prior to entering the PROCAS study were excluded from the current study, as were data from those women with additional mammographic views. PROCAS mammograms were in three different formats as shown in Table 1. Due to computational memory limitations, those with format C were excluded. The number of exclusions for all criteria (n=21299) are shown in Table 2 leaving data from 36606 women and 145820 mammographic images for analysis.

Table 1: Mammographic image formats in PROCAS

Format	**Dimensions (pixels)**	**Pixel Size** (μm)
A	2294×1914	94.1
B	3062×2394	94.1
C	5625×4095	54.0

Table 2: Exclusion table. [a]

Reason for exclusion	**Number Excluded**
Additional mammographic views	2384
Format C mammographic image size	6513
Previous diagnosis of cancer	1068
No FFDM	13400

[a] Some exclusions fall into more than one category

2.1 Training data

The training set was built by randomly selecting 50% of the data which met the inclusion and exclusion criteria. Data from all women that were included in the two case control test sets described in Section 2.3 were further removed from the training set to ensure no overlap between training and test sets. The training set consisted of 67520 images from 16968 women (132 cancers and 16836 non-cancers). A validation set comprising approximately 5% of the training set was used for parameter selection and to avoid over-fitting.

2.2 Model selection data

The model selection set consisted of data from the remaining 50% of women (73128 images from 18360 women, 393 cancers and 17967 non-cancers) that were not included in the training set. We used all four mammographic views and analysed data on a per mammogram and per woman basis (see Section 3.6). To ensure no overlap between model selection and test sets, all data included in the SDC and prior test sets were removed from the Model Selection set. The purpose of this set is to select the best model configuration in terms of VAS score prediction.

2.3 Test data

We evaluated our method using two datasets: the Screen-Detected Cancers (SDC) and prior datasets. The SDC and prior datasets are the same as those used by Astley et al.[14] In both test datasets control/non-cancer data was from women who had both a cancer-free (normal) mammogram at entry to PROCAS, and a subsequent cancer-free (normal) mammogram. Cancers were either detected at entry to PROCAS, as interval cancers or at subsequent screens.

SDC dataset

The SDC dataset was a subset of PROCAS with mammographic images from 1646 women (366 cancers and 1098 non-cancers). All cancers were detected during screening on entry to PROCAS. Mammographic density was assessed in the contralateral breast of women with cancer and in the same breast for the matched controls. Each case was matched to three controls based on age (+/-12 months), BMI category (missing, <24.9, 25.0-29.9, 30+ kg/m2), hormone replacement therapy (HRT) use (current *vs* never/ever) and menopausal status (premenopausal, perimenopausal or postmenopausal).

Prior dataset

The prior dataset consisted of 338 cancers and 1014 controls also from the PROCAS study. All cases in this dataset were cancer-free on entry to PROCAS but diagnosed subsequently. The median time to diagnosis of cancer was 36 months (25th percentile: 32 months, 75th percentile: 39 months). We analysed the mammographic images of these women on entry to PROCAS, using all four mammographic views. Similarly to the SDC dataset, cases were matched to three controls based on age, BMI category, HRT, menopausal status and year of mammogram.

3 METHOD

3.1 Visual assessment of density

In the PROCAS study, mammograms had their density assessed by two of nineteen independent readers (radiologists, advanced practitioner radiographers and breast physicians). The VAS used was a 10 cm line marked at the ends with 0% and 100%. Each reader marked their assessment of breast density on one scale for each mammographic view. Mammograms were assigned to readers

on a pragmatic basis. The VAS score for each mammographic image was computed as the average of the two reader scores. The VAS score per woman was averaged across all four mammographic images and across the two readers.

3.2 Deep learning model

We propose an automated method for assessing breast cancer risk based on whole-image full-field digital mammograms using reader VAS scores as a measure of breast density. As a first step, we built a deep CNN that takes whole-image mammograms as input and predicts a single number between 0 and 100. This number corresponds to the VAS score (percentage density). One of the main characteristics of CNNs is that features are learned from the training data without human input and are directly optimised for the prediction task. Features (often referred to as filters) are small patches which are convolved with the input image and create activation maps that show how the input responds to the filters. The values of the features are automatically adjusted to optimise an objective function; in this case, the minimisation of the squared difference between predicted and reader VAS scores. Our implementation uses the TensorFlow library.[37] Our network consists of 6 groups of 2 convolutional layers and a max pooling layer. Our architecture is VGG-like, although there are some differences regarding the depth of the network and the number of feature maps which were imposed by memory constraints. Fig. 1 shows a conceptual representation of the network, the complete architecture is shown in Fig. 2. We use a non-saturating non-linear activation function ReLU[38] after each convolutional layer and apply batch normalization[39] before ReLU.

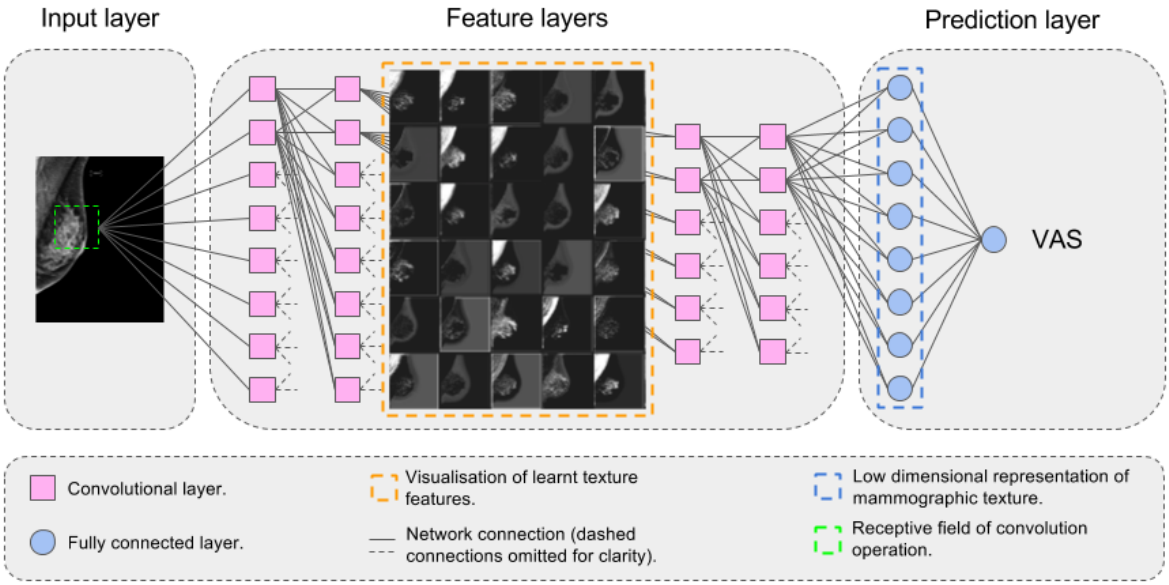

Fig 1: Conceptual diagram of our convolutional neural network for predicting VAS score.

3.3 Pre-processing

All mammographic images had the same spatial resolution. In order to have a single mammogram size, we padded format A mammograms with zeros on the bottom and right edges to match the image size of format B mammograms. Right breast mammograms were flipped horizontally before padding. Further, all mammograms were cropped to 2394x2995 and down-scaled using bicubic interpolation. Images were down-scaled due to memory limitations. We used two down-scaling factors to produce images of low and high resolution: 512x640 and 1024x1280 respectively. The upper bound of the pixel values was set to 75% of the pixel value range, to reduce the difference between background and breast pixel intensity. Finally, we inverted the pixel intensities and applied histogram equalisation (256 bins).[40] All pixel values were normalised in the range 0-1 before images were fed into the network. Table 3 shows the two input image formats used for training and their pixel size after down-scaling original images. No data augmentation techniques were applied to our dataset.

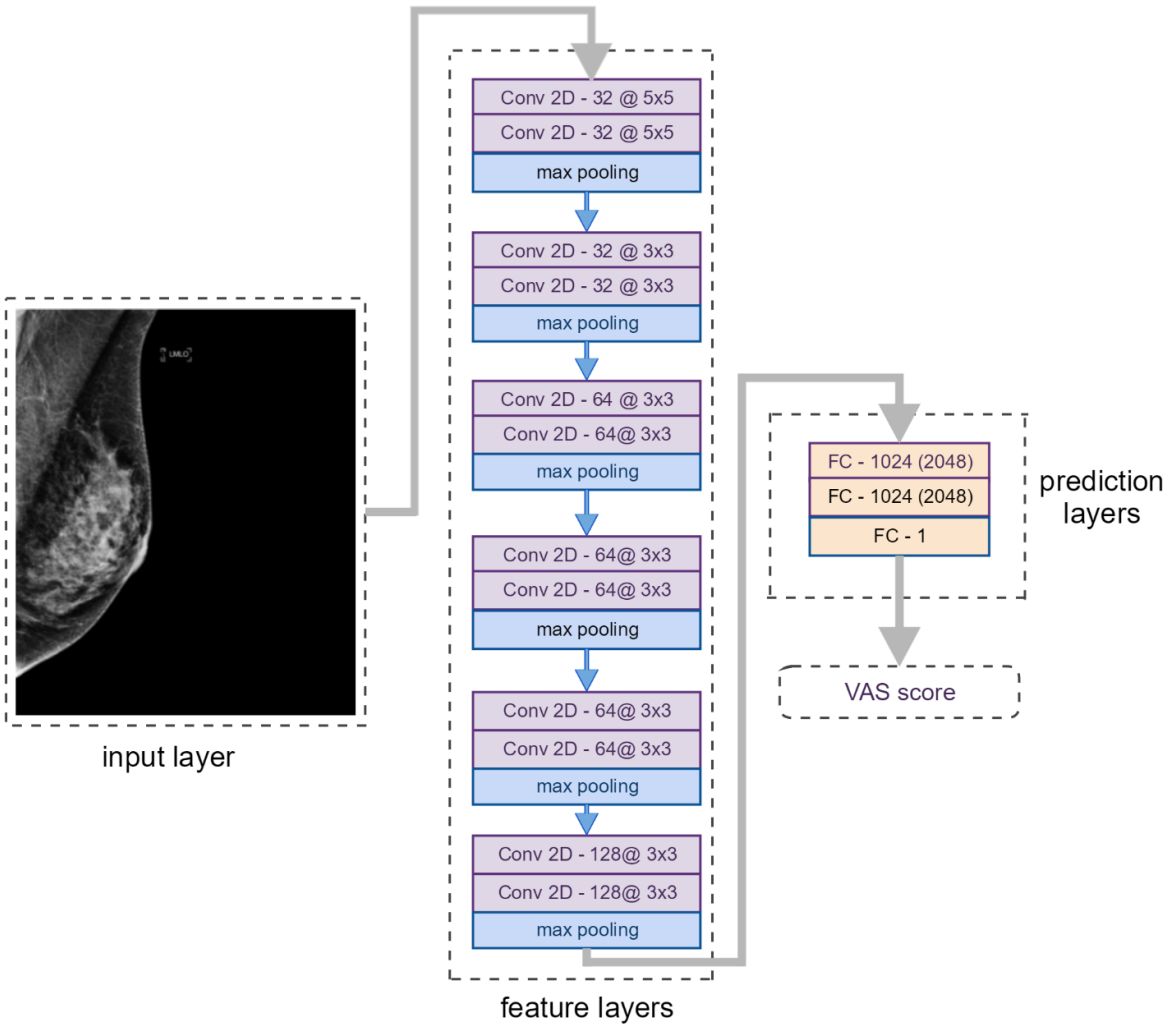

Fig 2: Network architecture and characteristics of each layer. The number of feature maps and the kernel size of each convolutional layer are shown as: feature maps@kernel size. The fully connected layers are marked with FC followed by the number of neurons in the layer for the low-resolution input and the number of neurons for the high-resolution input in parenthesis.

Table 3: Input image format used for training and pixel size after down-scaling original images

Format	**Dimensions (pixels)**	**Pixel Size** (μm)
Low resolution	640×512	20.12
High resolution	1240×1024	40.24

3.4 Training

We trained two independent networks, one for cranio-caudal (CC) images and one for medio-lateral oblique (MLO) images, using the architecture shown in Fig. 2. Each network takes pre-processed mammographic images as input and outputs a single value which represents a VAS score. We trained separate models for the two input size images. The CNN learns a mapping between the input mammographic image and the output VAS score. We used the Adam optimizer[41] with different values of initial learning rate: $5 \times 10^{-6}, 1 \times 10^{-6}, 5 \times 10^{-7}$ and 1×10^{-7}; we selected the models which performed best on the validation set. VAS scores do not have a uniform distribution across the population in PROCAS. The distribution is negatively skewed, over half of images have scores below 30% and only a fifth of images have scores above 50%, as shown in Fig. 3. Over-exposing our model to low VAS scores could skew the predicted values towards small VAS scores. To avoid this, we built balanced mini-batches by oversampling examples with high VAS scores. In the balanced mini-batch there is one example for each VAS value range of 20: 1 to 20, 21 to 40, etc. To assess the impact of the sampling strategy, we also trained the networks with randomly sampled mini-batches.

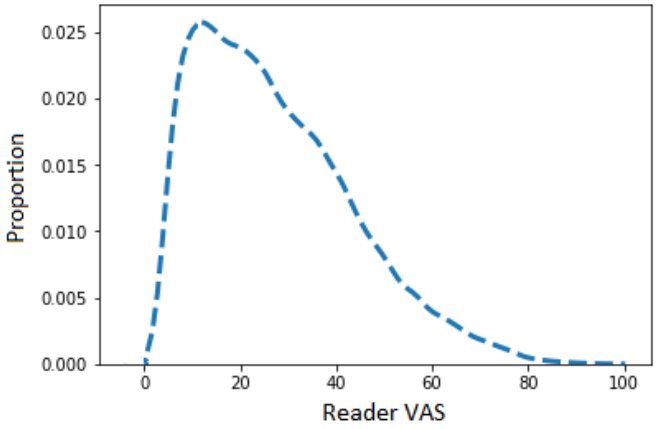

Fig 3: Distribution of VAS scores per image in PROCAS. The distribution is strongly skewed towards smaller values.

We trained the CNNs for 300,000 mini-batch iterations. Mini-batches consisted of 5 images. Weights were initialised with values from a normal distribution with 0 mean and standard deviation of 0.1. Biases were initialised with a value of 0.1. For the fully connected layers we used a dropout rate of 0.5 at training time. As described in Section 2.1, 5% of the training data was used as a validation set which was evaluated every 100 iterations, for early stopping. The best performing models on the validation set were evaluated on the model selection set. We used two cost functions: a mean squared error (MSE) and a weighted mean squared error. For the standard MSE, we computed loss as:

$$L = \frac{1}{n}\sum_{i=1}^{n}(Y_i - \hat{Y}_i)^2 \tag{1}$$

where Y is the vector of reader VAS, $\hat{Y}$ is the predicted VAS score. For the weighted function, each weight is inversely proportional to the inter-reader difference, so that examples where both readers agree, give a larger contribution to the loss:

$$L = \frac{1}{n}\sum_{i=1}^{n}\lambda_i(Y_i - \hat{Y}_i)^2 \tag{2}$$

where Y is the vector of reader VAS, $\hat{Y}$ is the predicted VAS score and λ is the absolute difference between two reader estimates. We have 8 different network configurations given by the input image size, sampling strategy and cost function. Table 4 shows their assigned names which will be used throughout the paper.

The low-resolution networks were trained on a Tesla P100 GPU whilst the high-resolution networks were trained on 4 Tesla P100 GPUs. Training time was approximately 36 hours for small resolution images and 6 days for high-resolution images.

Table 4: Networks configurations. Each configuration is a different combination of input size, cost function and sampling strategy. The low-resolution configurations have names starting with LR, and the high-resolution with HR. The cost function is reflected in the name as "w" for weighted cost function and "nw" for non-weighted. Finally, the sampling strategy adds "b" or "r" to the name, for balanced and random respectively.

Name	**Input size (pixels)**	**Cost function**	**Mini-batch sampling strategy**
LR-w-b	640×512	weighted MSE	balanced by VAS ranges of 20
LR-nw-b	640×512	MSE	balanced by VAS ranges of 20
LR-w-r	640×512	weighted MSE	random
LR-nw-r	640×512	MSE	random
HR-w-b	1240×1024	weighted MSE	balanced by VAS ranges of 20
HR-nw-b	1240×1024	MSE	balanced by VAS ranges of 20
HR-w-r	1240×1024	weighted MSE	random
HR-nw-r	1240×1024	MSE	random

3.5 Predicting density score

The MLO or CC network predicted a single VAS score for each previously unseen mammogram image. A small proportion of images (approximately 1%) produced a negative VAS score and were set to zero. The VAS score for a woman was computed by averaging scores across all mammogram images available (both breasts and both views).

3.6 Model selection & testing

Breast cancer risk prediction was assessed by first selecting the CNN architecture that gave the highest accuracy on the model selection set. The predicted VAS scores from this model were used to assess breast cancer risk on both the prior and SDC datasets.

Model selection

VAS scores per image and woman were predicted for low and high-resolution images for different parameter configurations (Table 4) for the model selection dataset, with the aim of selecting the

best performing model. MSE with bootstrap confidence intervals were calculated for each configuration. Additionally, Bland-Altman plots[42] were used to evaluate the agreement between reader and predicted VAS scores and to identify any systematic bias in predicted VAS. We computed the reproducibility coefficient (RPC) which quantifies the agreement between reader and predicted VAS. 95% of predicted VAS scores are expected to be within one RPC from the median after adjusting for systematic bias.

Prediction of breast cancer

To evaluate the selected model's ability to predict breast cancer we used the screen detected cancer (SDC) and prior datasets described in Section 2.3. For this we used only predicted VAS per woman which was calculated differently for the two datasets. For prior, scores for all views available were averaged. For the SDC set, only the contralateral side was used for cancer cases; for controls, we used the same side as their matched case.

The relationship between VAS and case-control status was analysed using conditional logistic regression with density measures modelled as quintiles based on the density distribution of controls. The difference in the likelihood-ratio chi-square between models with reader and predicted VAS scores was compared. The matched concordance (mC) index,[43] which provides a statistic similar to the area under the receiving operator characteristic curve (AUC) for matched case-control studies, was calculated with empirical bootstrap confidence intervals[43] to compare the discrimination performance of the models. All p-values are two-sided.

4 RESULTS

Model selection

For all network configurations and for both views, a learning rate of 5×10^{-6} was found to give the lowest MSE on the validation set. Table 5 and Table 6 show the MSE per image, per view and per woman obtained with different training strategies for the model selection set. The lowest MSE is obtained for the HR-nw-r configuration (high-resolution input, non-weighted cost function and random mini-batches) per image and HR-nw-b (high-resolution input, non-weighted cost function and balanced mini-batches) per woman. Overall, the high-resolution input configurations outperformed the corresponding low-resolution configurations by a small margin. Training with balanced mini batches increased the MSE in the majority of cases with the exception of HR-nw-b per woman and HR-w-b both per image and per woman. This may be because balancing mini-batches has the equivalent effect of increasing the weight of under-represented VAS labels in the cost function.

Table 5: Mean squared error (95% confidence intervals) for the model selection set, for the high-resolution images. Each column represents a different network configuration. The first row shows values obtained for the predictions made per image; the second and third row show MSE for CC and MLO respectively; the fourth row shows results averaged per woman.

	HR-nw-r	**HR-w-r**	**HR-nw-b**	**HR-w-b**
per image	96.1 (94.8 - 97.3)	106.5 (105.1 - 107.9)	99.2 (97.9 - 100.5)	104.1 (102.8 - 105.2)
CC	94.6 (93.0 - 96.3)	103.3 (101.4 - 105.2)	99.0 (97.3 - 100.8)	103.1 (101.5 - 104.8)
MLO	97.6 (95.8 - 99.5)	109.8 (107.6 - 111.9)	99.3 (97.5 - 101.0)	105.0 (103.1 - 106.9)
per woman	79.3 (77.2 - 81.3)	86.2 (84.0 - 88.7)	77.3 (75.4 - 79.3)	81.9 (79.8 - 84.1)

Fig. 4 (a) and (b) and show the MSE value per range of 10 values of reader VAS for low- and high-resolution input respectively. These plots show the impact of different training parameters on prediction error.

Table 6: Mean squared error (95% confidence intervals) for the model selection set, for the low-resolution images. Each column represents a different network configuration. The first row shows values obtained for the predictions made per image; the second and third row show MSE for CC and MLO respectively; the fourth row shows results averaged per woman.

	LR-nw-r	**LR-w-r**	**LR-nw-b**	**LR-w-b**
per image	98.0 (96.7 - 99.2)	108.4 (107.0 - 109.9)	104.0 (102.7 - 105.3)	113.3 (112.0 - 114.8)
CC	100.0 (98.2 - 101.7)	110.8 (108.8 - 112.8)	108.0 (106.2 - 109.8)	116.8 (114.8 - 118.6)
MLO	95.9 (94.1 - 97.7)	106.1 (104.1 - 108.3)	99.9 (97.9 - 101.8)	109.9 (108.0 - 111.7)
per woman	79.4 (77.3 - 81.4)	87.2 (84.8 - 89.7)	82.1 (80.0 - 84.3)	90.2 (88.0 - 92.4)

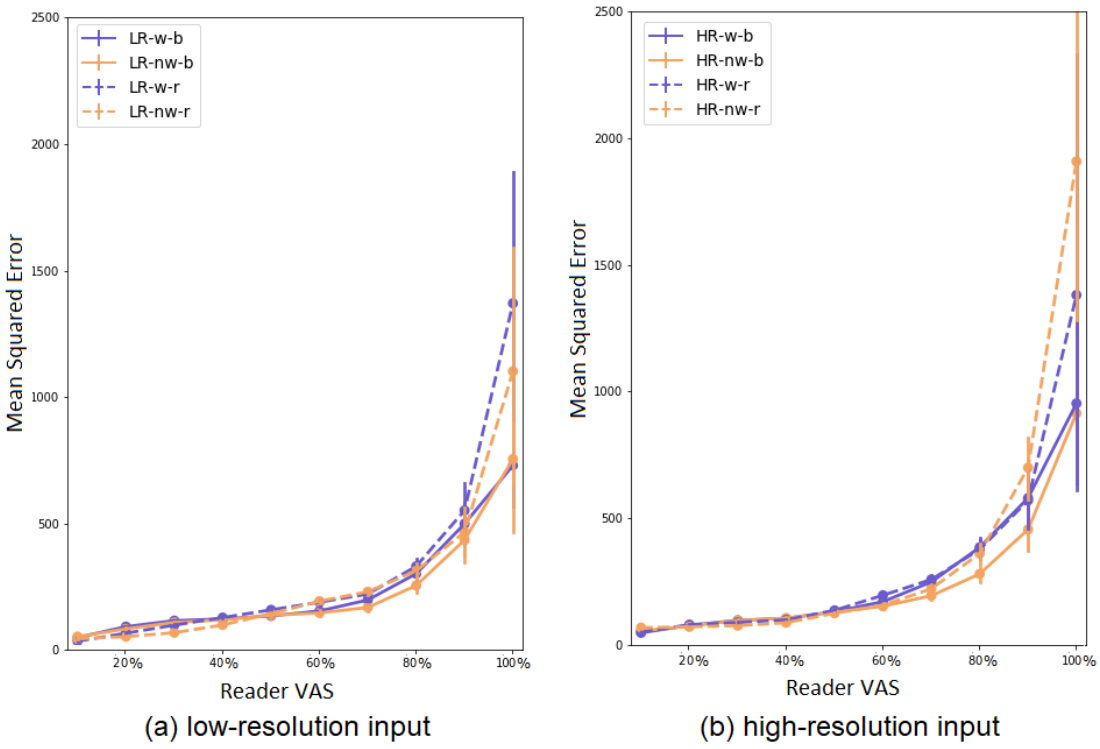

(a) low-resolution input (b) high-resolution input

Fig 4: MSE with 95% CI per image for low- and high-resolution input. All configurations are displayed with a different line style or colour. Configurations with weighted cost function are displayed in purple, and non-weighted in orange. Balanced mini-batches are displayed with a solid line, and random ones with dashed lines. Data were analysed in divisions of 10% of VAS score. The Y-axis shows the mean squared error of the predicted VAS score.

Using balanced mini-batches increased the error in the smaller values of VAS but decreased it for larger VAS values. The weighted cost function improves the error at the ends of the VAS range, where the inter-reader variability is low (shown in Fig. 5). The effects of balancing and weighted

cost function are less prominent for the high-resolution images. The reduced performance with balanced mini-batches may have been caused by the impact this weighting had on changing the distribution of VAS labels between training and test data. The weighted cost function also increased the MSE across all models. This cost function reduced the weight of those samples for which there is disagreement between two readers. Fig. 5 shows the distribution is heavily skewed towards the middle of the VAS range, thus the weighting of these samples would also change the distribution of VAS labels with respect to the test set. Similar plots for CC performance and MLO performance are shown in Fig. 6. Table 7 shows the mean squared difference between the two readers.

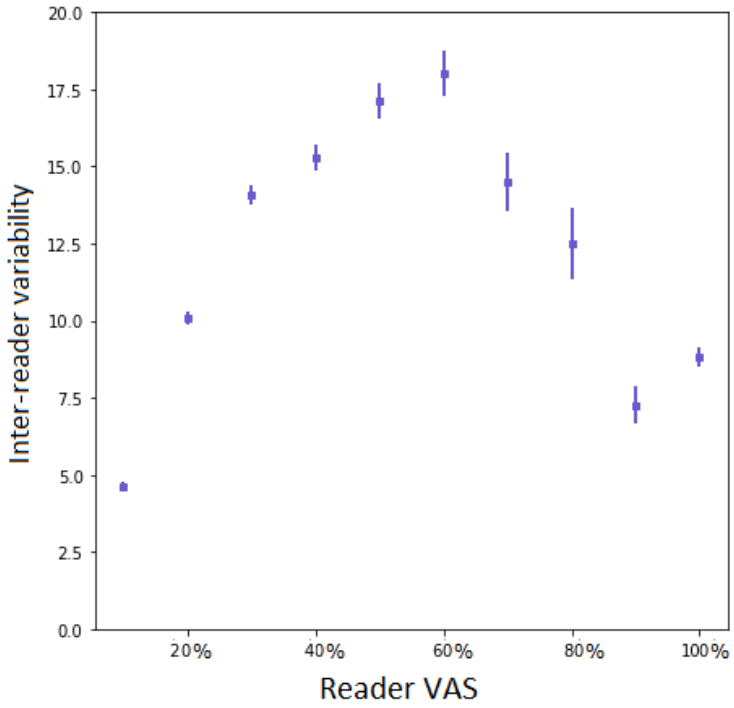

Fig 5: Plot of inter-reader variability with 95% CI for ranges of 10 values of reader VAS score. X-axis shows the ranges of reader VAS (average of two readers) and Y-axis shows the average inter-reader variability. Inter-reader variability is computed as the absolute difference between the scores of two readers for each mammographic image.

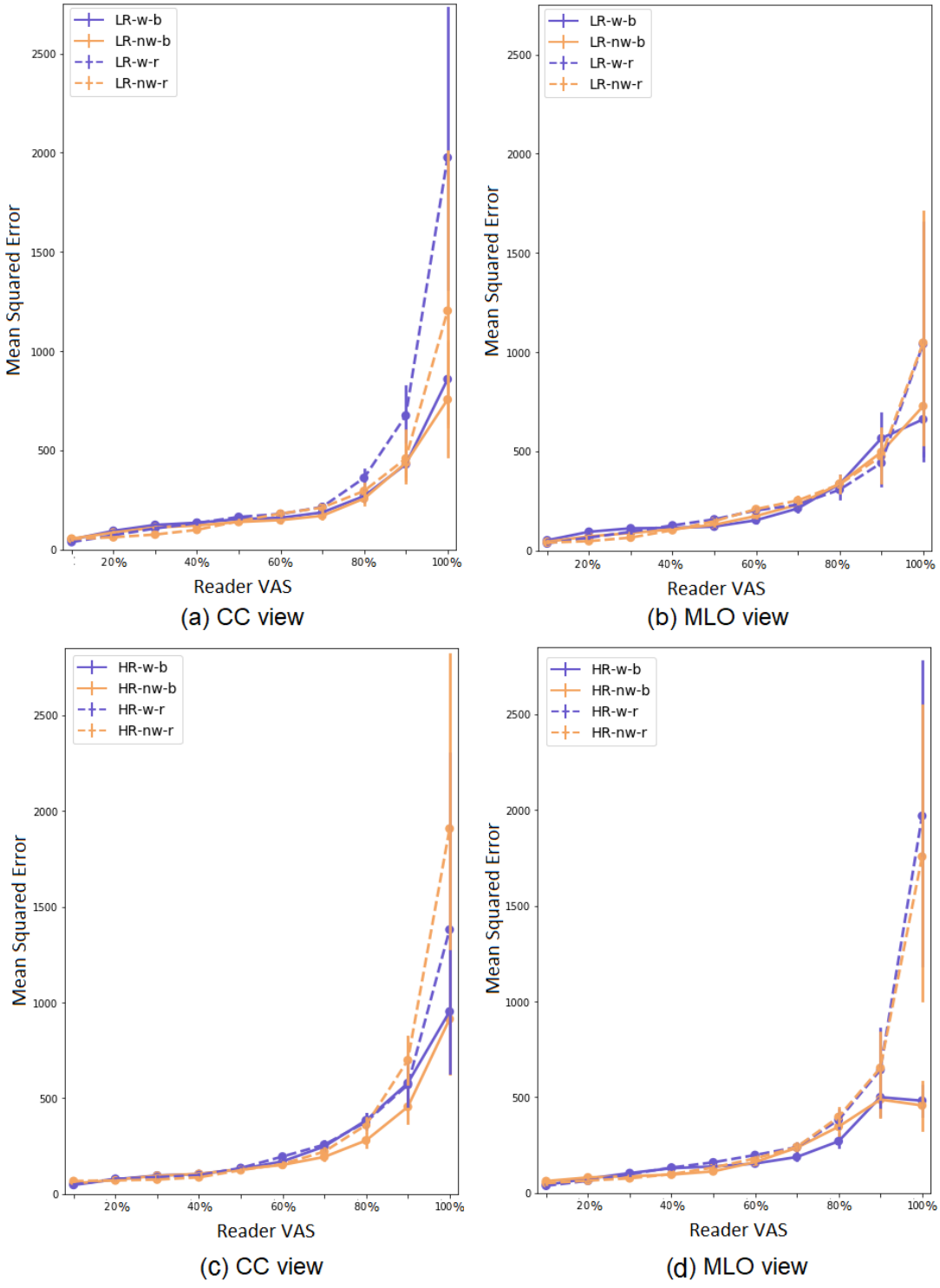

Fig 6: MSE with 95% CI per image for low- and high-resolution input for CC and MLO views. All configurations are displayed with a different line style or colour. Configurations with weighted cost function are displayed in purple, and non-weighted in orange. Balanced mini-batches are displayed with a solid line, and random ones with dashed lines. Data were analysed in divisions of 10% of VAS score. The Y-axis shows the mean squared error of the predicted VAS score. (a) and (b) show the MSE for low-resolution, (c) and (d) for high-resolution.

Table 7: Mean squared difference between readers

	MSE (95% CI)
per image	267.5 (264.4 - 270.9)
per woman	258.7 (252.6 - 264.6)

Plots of the inter-reader difference against predicted vs reader difference are shown in Fig. 7.

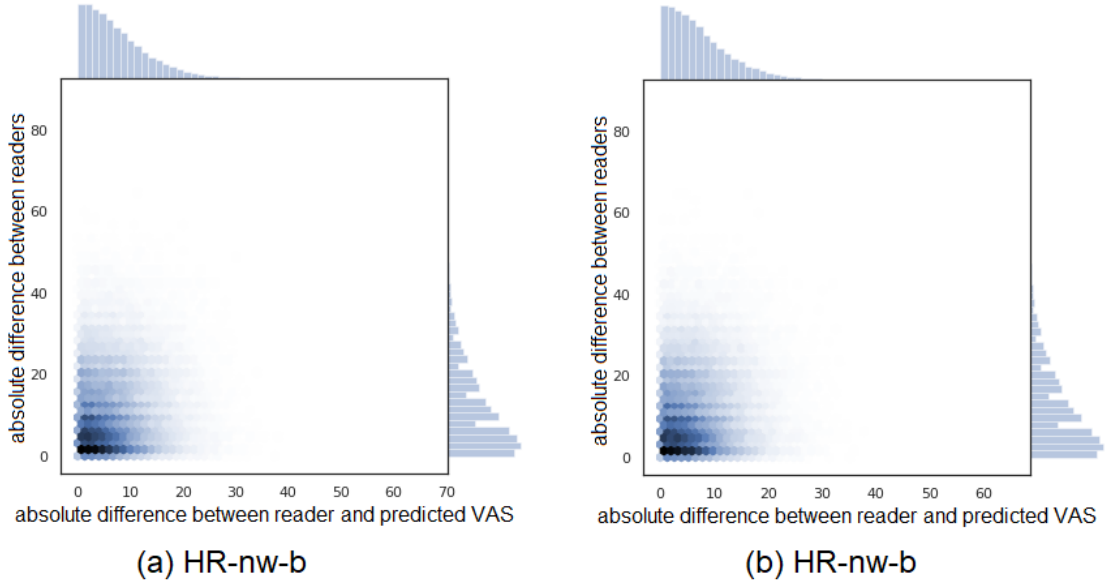

Fig 7: Plot of inter-reader absolute difference vs absolute difference between reader and predicted VAS on the model selection set for two models (a) HR-nw-b, (b) HR-nw-r.

For all configurations, Bland Altman analysis[42] showed good agreement between predicted VAS and reader scores. The reproducibility coefficient (RPC) for predicted VAS per mammographic image was $<$18.0% for high-resolution input and $<$19.0% for low-resolution input. When analysed on a 'per woman' basis, the RPC values were $<$16.0% and $<$16.3% for high- and low-resolution input respectively. Systematic bias was low across all configurations with values between -2.0% and 1.5% per image and between -1.5% and 1.3% per woman. Table 8 shows the Pearson correlation values for the model selection set and the two test sets. Bland-Altman plots of HR-nw-r and HR-nw-b for the model selection set are shown in Fig. 8.

Table 8: Correlation between predicted and reader VAS per image and per woman. All correlations have p<0.01

	dataset	HR-nw-r	HR-nw-b
per image	model selection set	0.805	0.803
	SDC	0.808	0.806
	prior	0.812	0.812
per woman	model selection set	0.838	0.843
	SDC	0.834	0.845
	prior	0.846	0.851

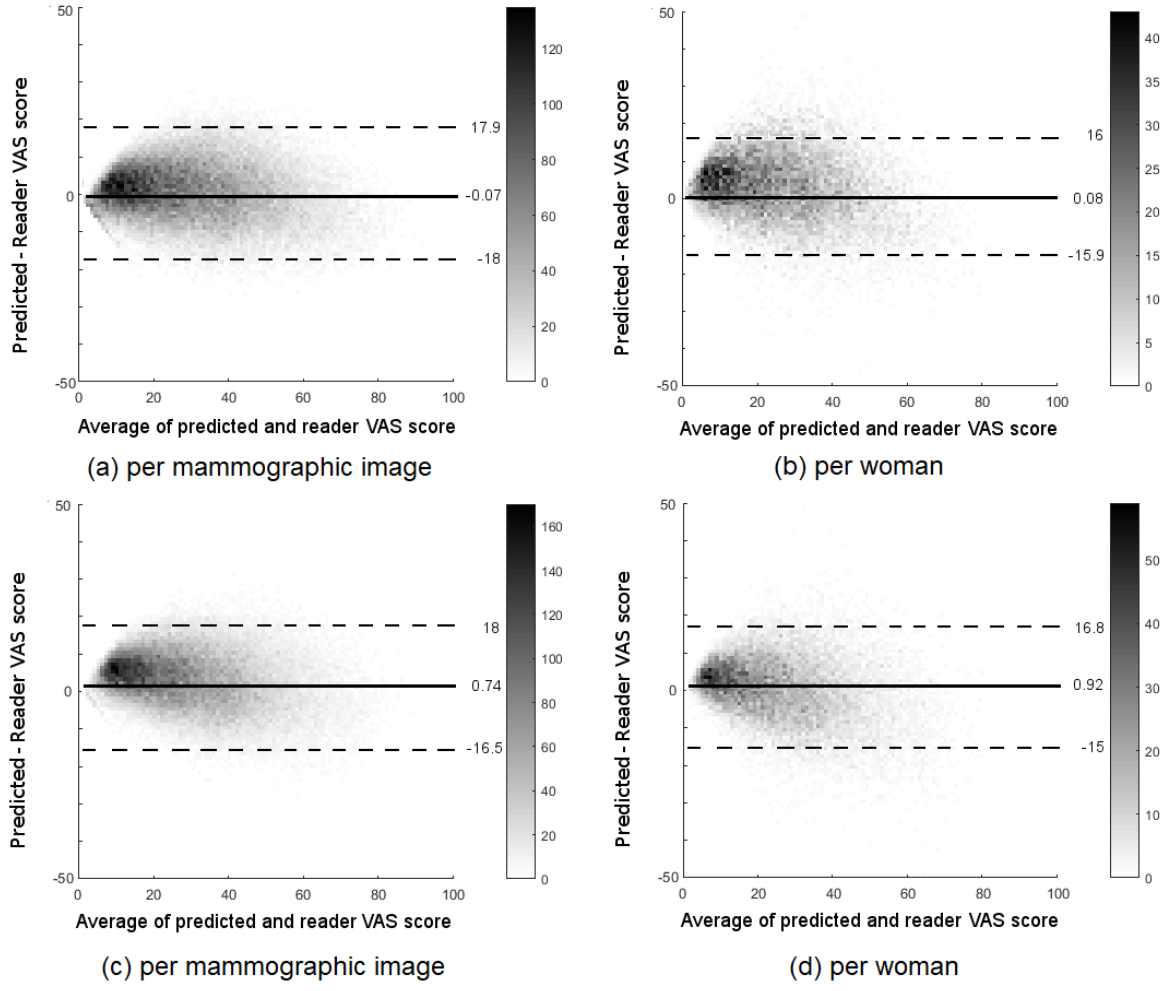

Fig 8: Bland-Altman plot of predicted and reader VAS score for the model selection set. The horizontal axis shows the average of reader and predicted VAS scores; the vertical axis shows the difference between predicted and reader VAS scores. Solid line represents median, dashed lines show the 95% confidence limits. The grey level of each point indicates the number of points as shown on the right hand side of each plot. (a) and (b) for Hr-nw-b, (c) and (d) for HR-nw-r.

Fig. 9 shows the reader scores plotted for all pairs of views. The Pearson correlation coefficient r varies between 0.97 and 0.99. Fig. 10 and Fig. 11 show the predicted scores for all pairs of views obtained with HR-nw-r and HR-nw-b respectively. The Pearson correlation coefficient r varies between 0.86 and 0.92 showing good agreement between scores across all four views.

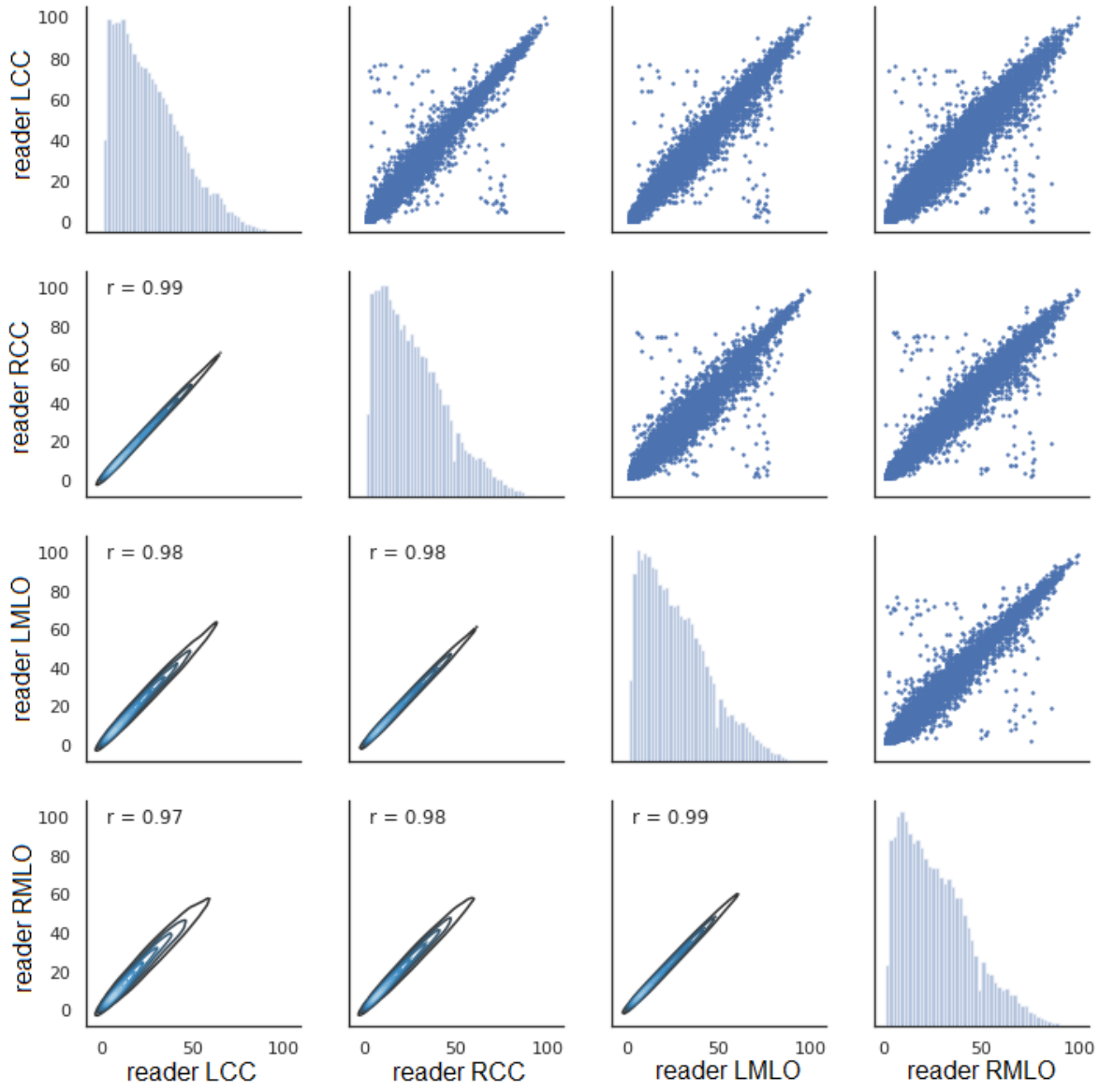

Fig 9: Scatter plot and density plots of reader scores for all pairs of views.

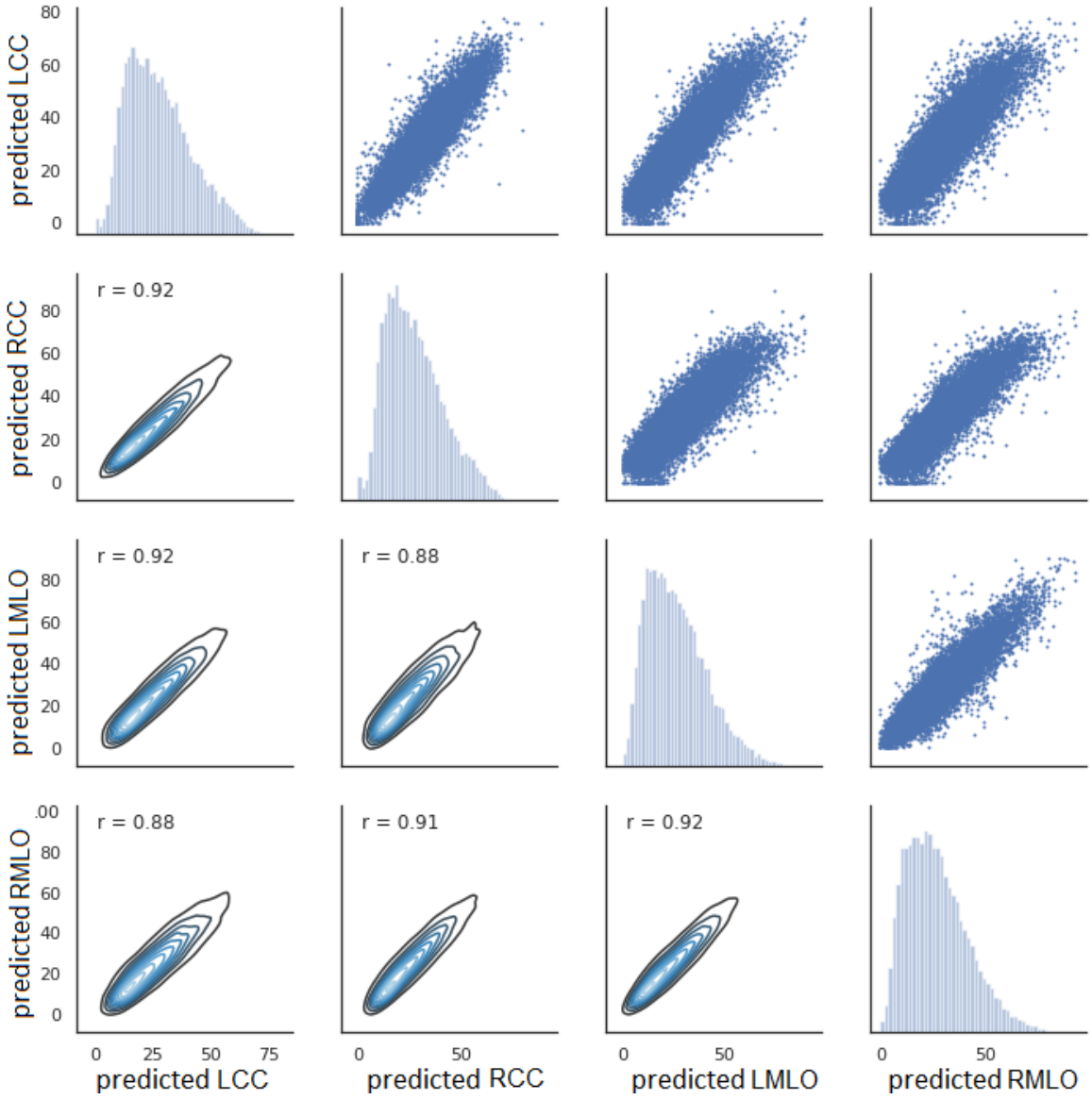

Fig 10: Scatter plot and density plots of predicted scores for HR-nw-r, for all pairs of views.

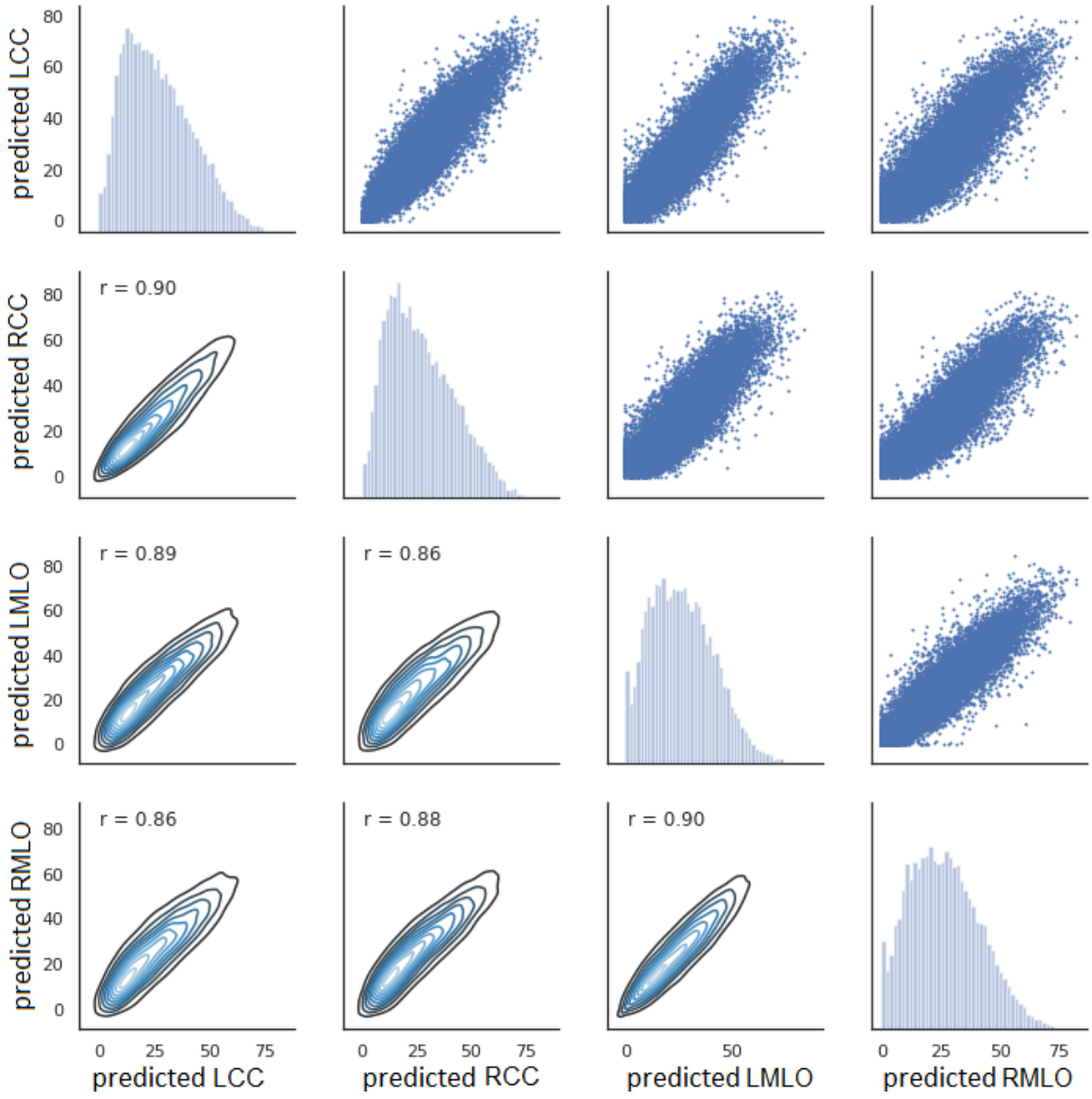

Fig 11: Scatter plot and density plots of predicted scores for HR-nw-b, for all pairs of views.

Prediction of breast cancer

Fig. 12 illustrates the odds of developing breast cancer for women in quintiles of predicted VAS score compared to women in the lowest quintile for the prior dataset. Table 9 shows the odds of developing breast cancer for women in the highest quintile of VAS score compared to women in the lowest quintile. Predicted and reader VAS both gave a statistically significant association with

breast cancer risk for the SDC and prior datasets. However, the odds ratio associated with reader VAS was higher than that for predicted VAS. For the SDC dataset, the odds ratio for women in the highest quintile compared to women in the lowest quintile of predicted VAS was 2.49 (95% CI: 1.57 - 3.96) for HR-nw-r and 2.40 (95% CI: 1.53 - 3.78) for HR-nw-b. In the prior dataset the OR for predicted VAS was 4.16 (95% CI: 2.53 - 6.82) for HR-nw-r and 4.06 (95% CI 2.51 - 6.56) for HR-nw-b.

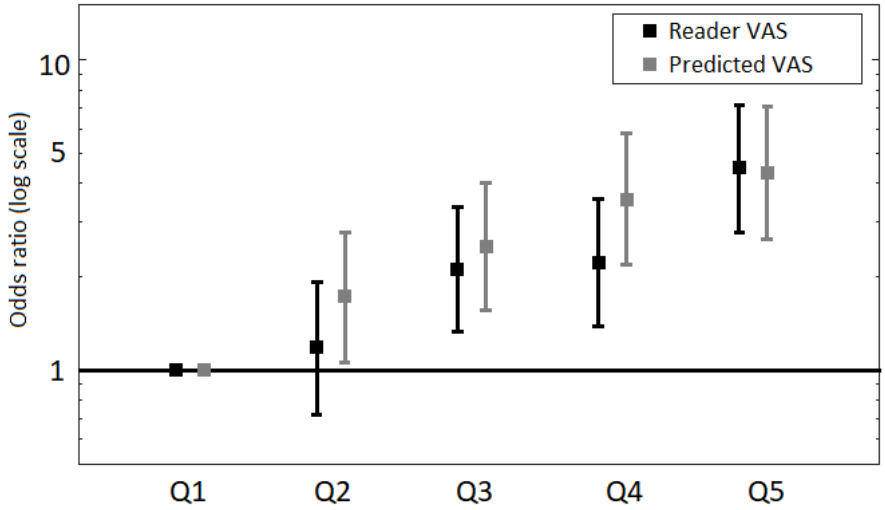

Fig 12: Odds of developing breast cancer with 95% CIs for reader and predicted VAS on the prior dataset. Predicted VAS is computed with the HR-nw-r model (high-resolution input, non-weighted cost function, random mini-batches).

Table 9: Odds ratio (95% CI) for highest quintile compared to lowest quintile of VAS scores for both case-control datasets

	Prior (OR, 95% CI)	**SDC (OR, 95% CI)**
Reader VAS	4.41 (2.76 - 7.06)	4.63 (2.82 - 7.60)
HR-nw-r	4.16 (2.53 - 6.82)	2.49 (1.57 - 3.96)
HR-nw-b	4.06 (2.51 - 6.56)	2.40 (1.53 - 3.78)

Table 10 shows the matched concordance index obtained for both case-control datasets. The matched concordance index for reader VAS was higher than predicted VAS for both datasets show-

ing better discrimination between cases and controls for reader VAS. Table 11 shows the p-values based on the likelihood ratio chi-square comparing the difference between models for each case-control dataset. In the SDC case control study, reader VAS was a significantly better predictor than predicted VAS for both HR-nw-r (p=0.002) and HR-nw-b (p=0.001). For the prior dataset, there was no significant difference between reader VAS and predicted VAS for HR-nw-r (p=0.134) but reader VAS was a better predictor than HR-w-b (p=0.041). There was no significant difference between HR-w-r and HR-w-b on either the prior (p=0.902) or SDC (p =0.760) datasets.

Table 10: Matched concordance index for predicted and reader VAS for both case-control datasets

	Prior (95% CI)	**SDC (95% CI)**
Reader VAS	0.642 (0.602 - 0.678)	0.645 (0.605 - 0.683)
HR-nw-r	0.616 (0.578 - 0.655)	0.587 (0.542 - 0.627)
HR-nw-b	0.624 (0.586 - 0.663)	0.589 (0.551 - 0.628)

Table 11: P-values based on likelihood ratio comparing different models

Model comparison	**Prior (p-values)**	**SDC (p-values)**
Reader *vs* HR-nw-r	p=0.134	p=0.002
Reader *vs* HR-w-b	p=0.041	p=0.001
HR-w-b *vs* HR-nw-r	p=0.902	p=0.760

Bland-Altman plots of HR-nw-r and HR-nw-b for the two case control sets are shown in Fig. 13 and Fig. 14.

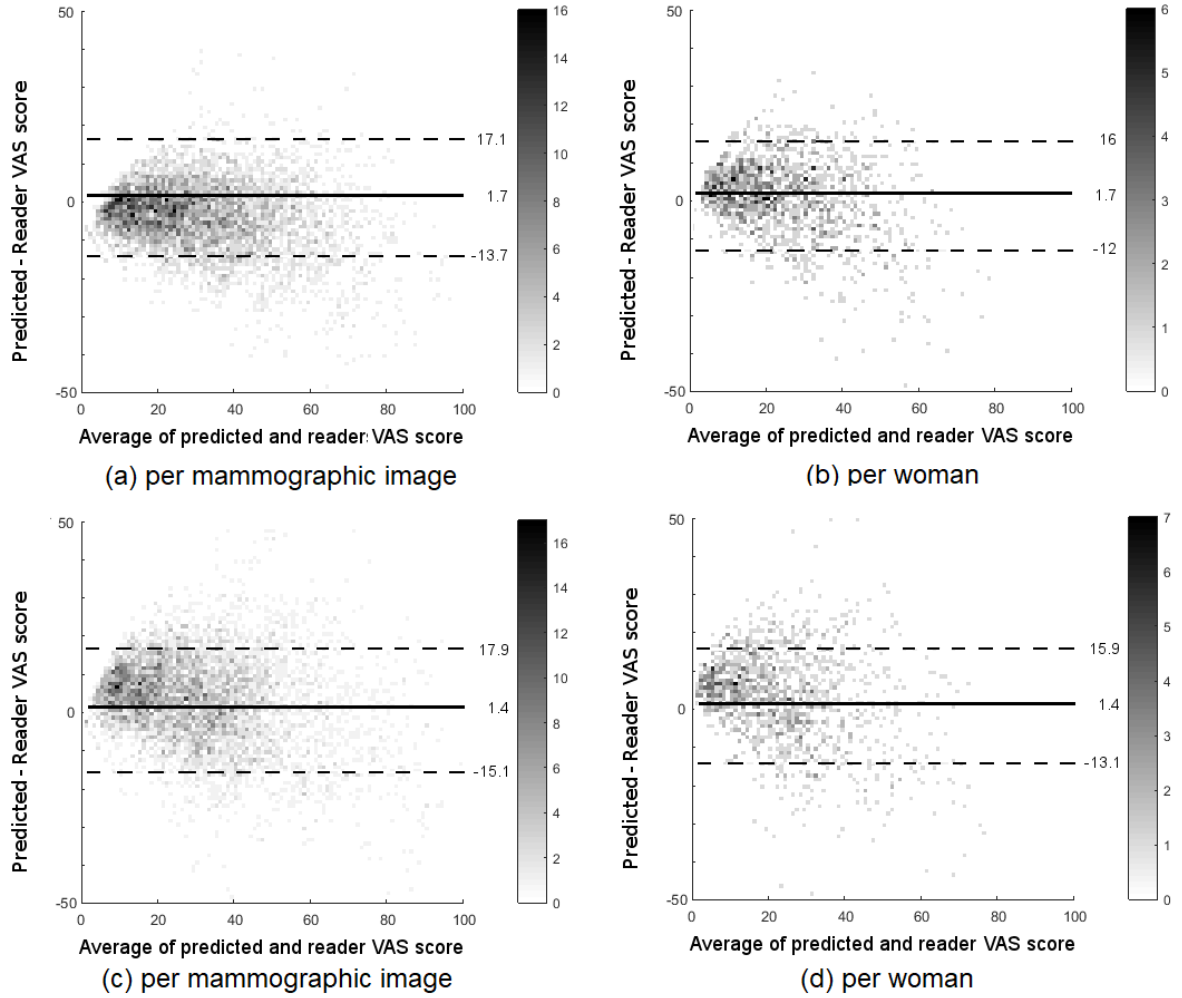

Fig 13: Bland-Altman plot of predicted and reader VAS score for the HR-nw-r model. The horizontal axis shows the average of reader and predicted VAS scores; the vertical axis shows the difference between predicted and reader VAS scores. Solid line represents median, dashed lines show the 95% confidence limits. The grey level of each point indicates the number of points as shown on the right hand side of each plot. (a) and (b) for the SDC set; (c) and (d) for the prior set.

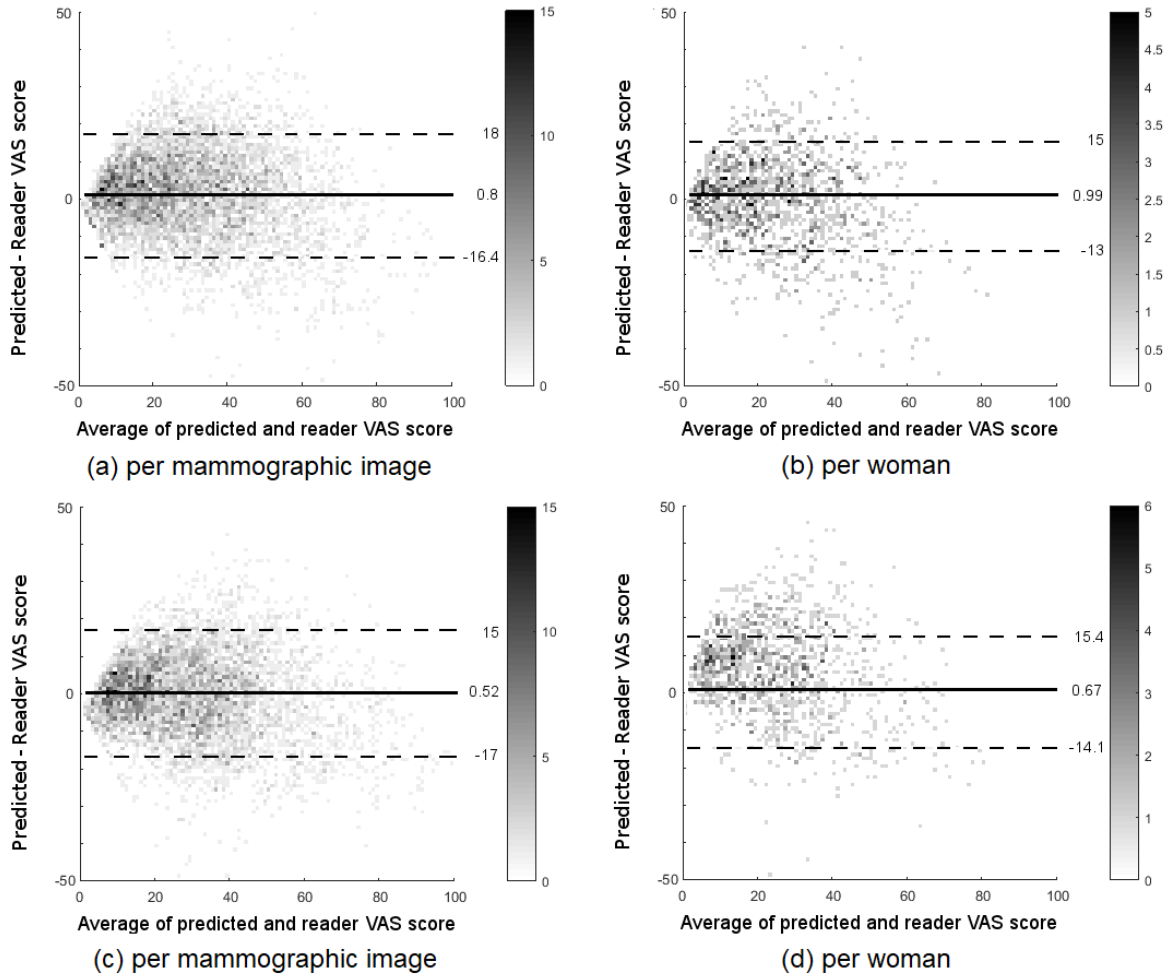

Fig 14: Bland-Altman plot of predicted and reader VAS score for the HR-nw-b model. The horizontal axis shows the average of reader and predicted VAS scores; the vertical axis shows the difference between predicted and reader VAS scores. Solid line represents median, dashed lines show the 95% confidence limits. The grey level of each point indicates the number of points as shown on the right hand side of each plot. (a) and (b) for the SDC set; (c) and (d) for the prior set.

5 Discussion

In this paper we present a fully automated method to predict VAS scores for breast density assessment. Breast density is an important risk factor for breast cancer, although studies vary in their findings regarding which breast density measure is most predictive of cancer. Recent studies have shown that automated methods are capable of matching radiologists' performance for breast density assessment. Kerlikowske et al.[44] compared automatic BI-RADS with clinical BI-RADS and

showed they similarly predicted both interval and screen-detected cancer risk, which indicates that either measure may be used for density assessment. A deep learning method proposed by Lehman et al.[45] for assessing BI-RADS density in a clinical setting, showed good agreement between the model's predictions and radiologists' assessments. Duffy et al.[46] investigated the association of different density measures with breast cancer risk using digital breast tomosynthesis and compared automatic and visual measures. All measures showed a positive correlation with cancer risk, but the strongest effect was shown by an absolute density measure. However, Astley et al.[14] showed that subjective assessment of breast density was a stronger predictor of breast cancer than other automated and semi-automated methods.

Our method is the first automated method to attempt to reproduce reader VAS scores as an assessment of breast cancer risk, with results showing performance comparable to reader estimates. We used a large dataset with 145,820 mammographic full-field digital mammograms from 36,606 women and tested our networks on two datasets. We showed that CNNs can predict a VAS score that reflects reader VAS as a first step towards building a model for cancer risk prediction. Results showed a strong agreement between reader VAS and predicted VAS for both low and high-resolution images. Bland-Altman analysis showed similar results for all network configurations and there was no substantial difference in performance between low and high-resolution images. The mean difference (systematic bias) between reader and predicted VAS was small, however 95% limits of agreement showed considerable variation, which has been found to be a problem in the visual assessment of breast density both within and between readers.[18]

We investigated our method's capacity to predict breast cancer in the datasets previously used

by Astley et al.[14] An important finding is that although there is not complete agreement between predicted and reader VAS, this doesn't hinder the capacity of our method to predict cancer. Our method performed well, both in predicting breast cancer in women with screen detected cancer using the contralateral breast, and in predicting the future development of the disease, however ORs for predicted VAS were lower than those for reader VAS on both case-control datasets.

For predicting the future development of breast cancer our method suggests a stronger association with breast cancer risk than other automated density methods (Volpara, Quantra and Densitas) as reported by Astley et al. using the same data sets. Matched concordance index analysis revealed that VAS scores predicted using our method are similar to reader VAS in terms of assessing cancer status on the prior set (compared to 0.64 for reader VAS, 0.616 and 0.624 for our method with overlapping confidence intervals). On the SDC set, our predicted scores produced slightly lower matched concordance indices (0.587 and 0.589 for our method, and 0.645 for Reader VAS). This might be due to the use of only two predicted VAS scores to compute the average for each woman, rather than four for the prior dataset. However, the ability to identify women at risk before cancer is detected (as in the prior dataset) is more relevant for screening stratification. In this context, our method can identify women at risk similarly to radiologists.

One limitation of our study is that we used mammographic images produced with acquisition systems from a single vendor (GE Senographe Essential mammography system). Future work includes extending the method to work with images produced by different systems. The strengths of this approach include the fact that the method requires no human input and the pre-processing step is minimal. Our method aims to encapsulate expert perception of features that are associated with risk but may not be captured by methods that estimate the quantity of fibroglandular tissue.

Predicted VAS is fully automatic so does not suffer from the limitations of reader assessment such as inter-reader variability[18] or variations in ability to identify women at higher risk of developing breast cancer.[19] This would make it a pragmatic solution for population-based stratified screening.

6 Disclosures

Dr Adam R. Brentnall and Dr Jack Cuzick receive a royalty from CRUK for licencing TC for commercial use. The PROCAS study was supported by the National Institute for Health Research (NIHR) under its Programme Grants for Applied Research programme (reference number RP-PG-0707-10031: Improvement in risk prediction, early detection and prevention of breast cancer) and Prevent Breast Cancer (references GA09-003 and GA13-006). The views expressed are those of the author(s) and not necessarily those of the NHS, the NIHR, or the Department of Health. Prof Evans, Dr Astley and Dr Harkness are supported by the NIHR Manchester Biomedical Research Centre. Otherwise no conflicts of interest, financial or otherwise, are declared by the authors.

Ethics approval for the PROCAS study was through the North Manchester Research Ethics Committee (09/H1008/81). Informed consent was obtained from all participants on entry to the PROCAS study.

7 Acknowledgements

We would like to thank the study radiologists, breast physicians and advanced practitioner radiographers for VAS reading. We would also like to thank the many radiographers in the screening programme and the study centre staff for recruitment and data collection. This paper presents independent research funded by NIHR under its Programme Grants for Applied Research programme

(reference number RP-PG-0707-10031: “Improvement in risk prediction, early detection and prevention of breast cancer”) with additional funding from the Prevent Breast Cancer Appeal and supported by the NIHR Manchester Biomedical Research Centre. The views expressed are those of the author(s) and not necessarily those of the NHS, the NIHR, or the Department of Health.

We would like to thank the women who agreed to take part in the study, the study radiologists and advanced radiographic practitioners, and the study staff for recruitment and data collection.

Preliminary results obtained with the method described in this paper have been published in a previous paper: “Using a convolutional neural network to predict readers’ estimates of mammographic density for breast cancer risk assessment”.[47]

References

1 C. Huo, G. Chew, K. Britt, *et al.*, “Mammographic density - a review on the current understanding of its association with breast cancer,” *Breast cancer research and treatment* **144**(3), 479–502 (2014).

2 A. R. Brentnall, E. F. Harkness, S. M. Astley, *et al.*, “Mammographic density adds accuracy to both the Tyrer-Cuzick and Gail breast cancer risk models in a prospective UK screening cohort,” *Breast Cancer Research* **17**(1), 147 (2015).

3 J. Cuzick, J. Forbes, R. Edwards, *et al.*, “First results from the International Breast Cancer Intervention Study (IBIS-I): a randomised prevention trial.,” *Lancet (London, England)* **360**(9336), 817–824 (2002).

4 A. A. Mohamed, Y. Luo, H. Peng, *et al.*, “Understanding clinical mammographic breast density assessment: a deep learning perspective,” *Journal of digital imaging* , 1–6 (2017).

5 I. T. Gram, E. Funkhouser, and L. Tabár, "The tabar classification of mammographic parenchymal patterns," *European journal of radiology* **24**(2), 131–136 (1997).

6 B. Weber, J. Hayes, and W. P. Evans, "Breast density and the importance of supplemental screening," *Current Breast Cancer Reports* **10**(2), 122–130 (2018).

7 C. J. D'orsi, L. W. Bassett, W. A. Berg, *et al.*, "Breast imaging reporting and data system: ACR BI-RADS-mammography," *American College of Radiology* **4** (2003).

8 N. F. Boyd, H. Guo, L. J. Martin, *et al.*, "Mammographic density and the risk and detection of breast cancer," *New England Journal of Medicine* **356**(3), 227–236 (2007).

9 J. C. Sergeant, J. Warwick, D. G. Evans, *et al.*, "Volumetric and area-based breast density measurement in the predicting risk of cancer at screening (PROCAS) study," in *International Workshop on Digital Mammography*, 228–235, Springer (2012).

10 J. W. Byng, N. Boyd, E. Fishell, *et al.*, "The quantitative analysis of mammographic densities," *Physics in medicine and biology* **39**(10), 1629 (1994).

11 M. Abdolell, T. Hope, S. Zaboli, *et al.*, "Methods and systems for determining breast density," (2016). US Patent App. 14/912,965.

12 R. Highnam, S. M. Brady, M. J. Yaffe, *et al.*, "Robust breast composition measurement - volpara^{TM}," in *Proceedings of the 10th International Conference on Digital Mammography, IWDM'10*, 342–349, Springer-Verlag, (Berlin, Heidelberg) (2010).

13 S. Pahwa, S. Hari, S. Thulkar, *et al.*, "Evaluation of breast parenchymal density with quantra software," *The Indian journal of radiology & imaging* **25**(4), 391 (2015).

14 S. M. Astley, E. F. Harkness, J. C. Sergeant, *et al.*, "A comparison of five methods of measuring mammographic density: a case-control study," *Breast Cancer Research* **20**(1), 10 (2018).

15 A. Eng, Z. Gallant, J. Shepherd, *et al.*, "Digital mammographic density and breast cancer risk: a case–control study of six alternative density assessment methods," *Breast cancer research* **16**(5), 439 (2014).

16 J. J. James, F. J. Gilbert, M. G. Wallis, *et al.*, "Mammographic features of breast cancers at single reading with computer-aided detection and at double reading in a large multicenter prospective trial of computer-aided detection: CADET II," *Radiology* **256**(2), 379–386 (2010).

17 C. Wang, A. R. Brentnall, J. Cuzick, *et al.*, "A novel and fully automated mammographic texture analysis for risk prediction: results from two case-control studies," *Breast Cancer Research* **19**(1), 114 (2017).

18 J. C. Sergeant, L. Walshaw, M. Wilson, *et al.*, "Same task, same observers, different values: the problem with visual assessment of breast density," in *Medical Imaging 2013: Image Perception, Observer Performance, and Technology Assessment*, **8673**, 86730T, International Society for Optics and Photonics (2013).

19 M. Rayner, E. F. Harkness, P. Foden, *et al.*, "Reader performance in visual assessment of breast density using visual analogue scales: are some readers more predictive of breast cancer?," in *Medical Imaging 2018: Image Perception, Observer Performance, and Technology Assessment*, **10577**, 105770W, International Society for Optics and Photonics (2018).

20 M. G. Kallenberg, M. Lokate, C. H. Van Gils, *et al.*, "Automatic breast density segmentation: an integration of different approaches," *Physics in Medicine & Biology* **56**(9), 2715 (2011).

21 J. J. Heine, M. J. Carston, C. G. Scott, *et al.*, "An automated approach for estimation of breast density," *Cancer Epidemiology and Prevention Biomarkers* **17**(11), 3090–3097 (2008).

22 S. Petroudi, T. Kadir, and M. Brady, "Automatic classification of mammographic parenchymal patterns: A statistical approach," in *Engineering in Medicine and Biology Society*, **1**, 798–801 (2003).

23 G. Litjens, T. Kooi, B. E. Bejnordi, *et al.*, "A survey on deep learning in medical image analysis," *Medical image analysis* **42**, 60–88 (2017).

24 A. Krizhevsky, I. Sutskever, and G. E. Hinton, "ImageNet classification with deep convolutional neural networks," in *Advances in Neural Information Processing Systems 25*, 1097–1105, Curran Associates, Inc. (2012).

25 R. Girshick, J. Donahue, T. Darrell, *et al.*, "Rich feature hierarchies for accurate object detection and semantic segmentation," in *The IEEE Conference on Computer Vision and Pattern Recognition (CVPR)*, (2014).

26 H. R. Roth, C. T. Lee, H.-C. Shin, *et al.*, "Anatomy-specific classification of medical images using deep convolutional nets," *IEEE 12th International Symposium on Biomedical Imaging (ISBI)* , 101 – 104.

27 A. Dubrovina, P. Kisilev, B. Ginsburg, *et al.*, "Computational mammography using deep neural networks," *Computer Methods in Biomechanics and Biomedical Engineering: Imaging & Visualization* , 1–5 (2018).

28 N. Dhungel, G. Carneiro, and A. P. Bradley, "Automated mass detection in mammograms using cascaded deep learning and random forests," in *Digital Image Computing: Techniques and Applications (DICTA), 2015 International Conference on*, 1–8, IEEE (2015).

29 A. R. Jamieson, K. Drukker, and M. L. Giger, "Breast image feature learning with adaptive

deconvolutional networks," in *Medical Imaging 2012: Computer-Aided Diagnosis*, **8315**, 831506, International Society for Optics and Photonics (2012).

30 N. Dhungel, G. Carneiro, and A. P. Bradley, "Deep learning and structured prediction for the segmentation of mass in mammograms," in *International Conference on Medical Image Computing and Computer-Assisted Intervention*, 605–612, Springer (2015).

31 J.-Z. Cheng, D. Ni, Y.-H. Chou, *et al.*, "Computer-aided diagnosis with deep learning architecture: applications to breast lesions in us images and pulmonary nodules in CT scans," *Scientific reports* **6** (2016).

32 J. Wang, X. Yang, H. Cai, *et al.*, "Discrimination of breast cancer with microcalcifications on mammography by deep learning," *Scientific reports* **6** (2016).

33 K. Petersen, K. Chernoff, M. Nielsen, *et al.*, "Breast density scoring with multiscale denoising autoencoders," in *Proceedings of the STMI Workshop at the 15th International Conference on Medical Image Computing and Computer Assisted Intervention (MICCAI12)*, (2012).

34 M. Kallenberg, K. Petersen, M. Nielsen, *et al.*, "Unsupervised deep learning applied to breast density segmentation and mammographic risk scoring," *IEEE transactions on medical imaging* **35**(5), 1322–1331 (2016).

35 A. A. Mohamed, W. A. Berg, H. Peng, *et al.*, "A deep learning method for classifying mammographic breast density categories," *Medical physics* **45**(1), 314–321 (2018).

36 D. G. R. Evans *et al.*, "Assessing individual breast cancer risk within the u.k. national health service breast screening program: A new paradigm for cancer prevention," *Cancer Prevention Research* **5**(7), 943–951 (2012).

37 M. Abadi *et al.*, "TensorFlow: Large-scale machine learning on heterogeneous systems," (2015). Software available from tensorflow.org.

38 V. Nair and G. E. Hinton, "Rectified linear units improve restricted boltzmann machines," (2010).

39 S. Ioffe and C. Szegedy, "Batch normalization: Accelerating deep network training by reducing internal covariate shift," in *Proceedings of the 32nd International Conference on Machine Learning*, **37**, 448–456, PMLR, (Lille, France) (2015).

40 J. S. Lim, "Two-dimensional signal and image processing," *Englewood Cliffs, NJ, Prentice Hall* , 710 (1990).

41 D. P. Kingma and J. L. Ba, "Adam: A method for stochastic optimization," in *Proceedings of the 3rd International Conference for Learning Representations*, (2014).

42 D. G. Altman and J. M. Bland, "Measurement in medicine: the analysis of method comparison studies," *The statistician* , 307–317 (1983).

43 A. R. Brentnall, J. Cuzick, J. Field, *et al.*, "A concordance index for matched case–control studies with applications in cancer risk," *Statistics in medicine* **34**(3), 396–405 (2015).

44 K. Kerlikowske, C. Scott, A. Mahmoudzadeh, *et al.*, "Automated and clinical breast imaging reporting and data system density measures predict risk of screen-detected and interval cancers.," *Annals of internal medicine* (2018).

45 C. D. Lehman, A. Yala, T. Schuster, *et al.*, "Mammographic breast density assessment using deep learning: clinical implementation," *Radiology* , 180694 (2018).

46 S. W. Duffy, O. W. Morrish, P. C. Allgood, *et al.*, "Mammographic density and breast cancer

risk in breast screening assessment cases and women with a family history of breast cancer," *European Journal of Cancer* **88**, 48–56 (2018).

47 G. V. Ionescu, M. Fergie, M. Berks, *et al.*, "Using a convolutional neural network to predict readers' estimates of mammographic density for breast cancer risk assessment," in *14th International Workshop on Breast Imaging (IWBI 2018)*, **10718**, 107180D, International Society for Optics and Photonics (2018).

List of Figures

List of Tables